ACS OMEGA

Open Access

http://pubs.acs.org/journal/acsodf

Article

Mechanistic Studies on the Gold-Catalyzed Intramolecular Hydroalkylation of Ynamides to Indenes

Julien Annibaletto, Clément Jacob, Pierre Thilmany, Anaïs Loison, Jorge Escorihuela,* and Gwilherm Evano*

Cite This: *ACS Omega* 2024, 9, 51690−51700

Read Online

ACCESS | Metrics & More | Article Recommendations | Supporting Information

ABSTRACT: An in-depth experimental and computational study to rationalize the mechanism underlying the gold-catalyzed intramolecular hydroalkylation of ynamides to indenes is reported. Evaluating the reactivity of a set of deuterated ynamides and gold complexes allowed to get valuable insights into the mechanism of this reaction, while DFT calculations allowed to determine a plausible reaction pathway for this unprecedented transformation. This pathway involves the activation of the ynamide followed by a [1,5]-hydride shift from the highly reactive, in situ generated keteniminium ion, and a subsequent cyclization before deprotonation followed by a final protodeauration. According to DFT calculations, the initial [1,5]-hydride shift was identified as the rate-determining step of the reaction mechanism. Additionally, computational studies allowed to rationalize the differences in reactivity of various ynamides and the pivotal role of gold complexes in the catalysis of this reaction.

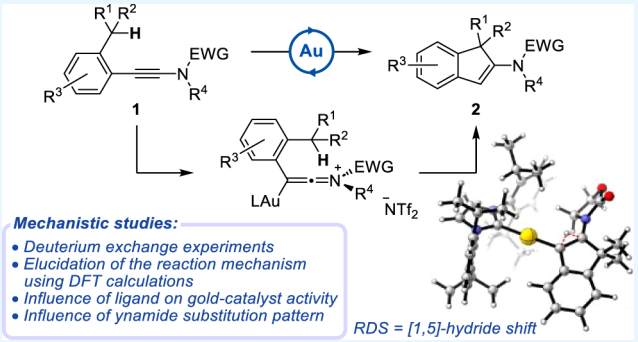

INTRODUCTION

Indenes are especially attractive targets in organic synthesis due to their widespread occurrence in biologically active molecules and their applications in many areas of science. This scaffold can indeed be found at the core structure of a range of naturally occurring molecules displaying antitumoral,[1] antimicrobial[2] and fungicidal[3] activities, among many others. These bicyclic fused carbocycles have in addition found a variety of applications in materials science as well, for instance in the fields of solar cells[4] and fluorescent materials.[5] They are also useful ligands in organometallic chemistry, as highlighted by the use of transition metal-indenyl complexes for the preparation of many small molecular scaffolds[6] and its application to the development of efficient polymerization processes.[7] An impressive array of methods has therefore been developed for their synthesis, enabling the preparation of a broad variety of indenes with various substituents and substitution patterns and from a variety of starting materials.[8] The two most common and general approaches rely on intramolecular Friedel−Crafts type and transition-metal catalyzed reactions, starting from bifunctional substrates containing an arene and an alkene, an allene, an alkyne or a propargylic alcohol. In the case of transition-metal catalyzed indene syntheses, most processes reported to date rely either on a C(sp^2)−H activation of the arene in the starting material with palladium or rhodium complexes, or on the activation of the double/triple bond by π-acidic gold complexes. Recently, gold catalysis could be successfully and elegantly extended to the activation of ynamides,[9] versatile building blocks in organic synthesis,[10] which notably led us to develop a novel synthesis of 2-amino-indenes **2**[11] based on a formal gold-catalyzed intramolecular hydroalkylation from suitably substituted ynamides **1**.[12]

This reaction proved efficient and enabled the synthesis of a variety of 2-amino-indenes from readily available ynamides under practical and user-friendly conditions since the cyclization only requires catalytic amounts of a NHC-gold catalyst, IPrAuNTf_2, overnight at room temperature in dichloromethane. Its mechanism however remains rather elusive. The most probable mechanistic scenario would first involve the generation of a highly reactive keteniminium ion **3**[13] upon activation of the starting ynamide **1** by the gold catalyst followed by [1,5]-hydride shift[14] leading to a benzylic carbocation **4**, which could trigger a subsequent cyclization and a final [1,2]-hydride shift or a deprotonation followed by protodeauration, ultimately affording 2-aminoindene **2** after release of the cationic gold species (Scheme 1). This proposed

Received: November 1, 2024
Revised: December 3, 2024
Accepted: December 5, 2024
Published: December 17, 2024

Scheme 1. Potential Mechanism Involved in the Synthesis of Indenes via a Gold-Catalyzed Intramolecular Hydroalkylation of Ynamides

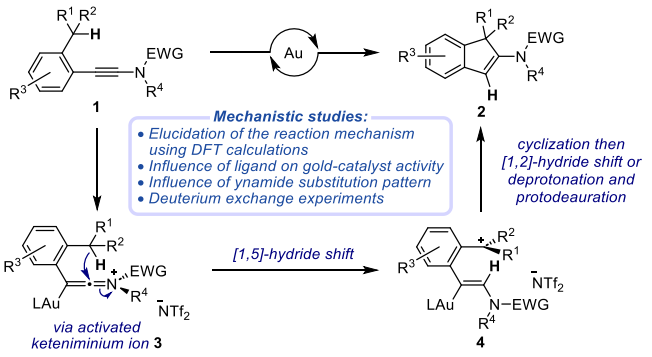

mechanism is however fully speculative and we now report extensive mechanistic studies based on a combined experimental and theoretical approach leading to a precise overview of the reaction mechanism and enabling the rationalization of the observed reactivity.

RESULTS AND DISCUSSION

Deuterium Labeling Experiments. Our study was initiated with deuterium labeling experiments to probe the intramolecular nature of the hydride transfer. In this perspective, deuterated ynamide $\mathbf{1a_D}$, bearing a deuterium atom at the benzylic position, was first prepared (Scheme 2).

Scheme 2. Synthesis of Deuterium-Labelled Ynamide $\mathbf{1a_D}$

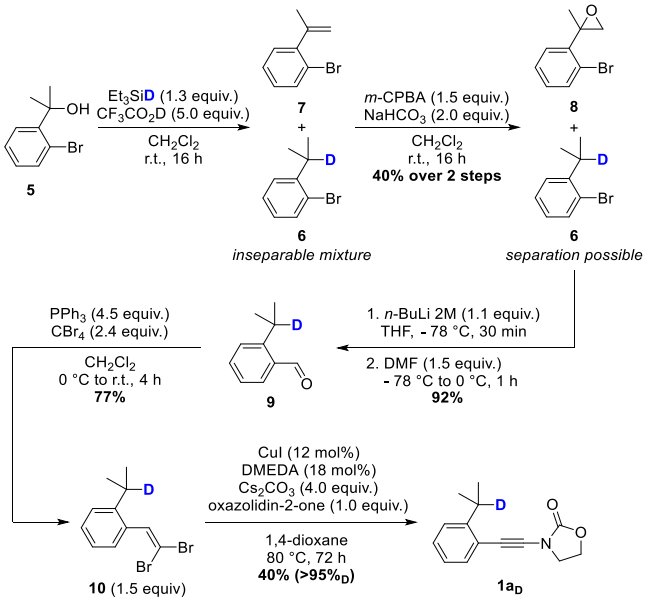

The synthesis of this substrate starts from commercially available bromobenzyl alcohol derivative **5**, which, upon reaction under reductive deoxygenation with a combination of deuterated trifluoroacetic acid and triethylsilane, provided an inseparable mixture of the desired deuterated substrate **6** along with styrene derivative **7**, resulting from a competing elimination under acidic conditions. A subsequent treatment of this mixture with *meta*-chloroperbenzoic acid enabled the epoxidation of undesired alkene **7** to the corresponding epoxide **8**, which could be separated from the desired deuterated compound **6** at this stage. Formylation of this compound through a bromine−lithium exchange upon reaction with *n*-butyllithium and subsequent trapping with DMF next afforded the corresponding aldehyde **9** without erosion of the deuterium content, which was next converted to *gem*-dibromoalkene **10** by a Ramirez olefination. A final copper-catalyzed cross-coupling reaction with oxazolidine-2-one under our previously reported conditions[15] using a combination of copper(I) iodide and *N*,*N*′-dimethylethylenediamine (DMEDA) as the ligand in the presence of cesium carbonate finally gave the desired ynamide $\mathbf{1a_D}$ with an excellent deuteration level (>95%$_D$).

With this ynamide $\mathbf{1a_D}$ selectively deuterated at the position from which the [1,5]-hydride shift would occur, we next engaged it under our optimized conditions for the intramolecular hydroalkylation involving 5 mol % of the gold catalyst IPrAuNTf$_2$ in dichloromethane at room temperature for 20 h (Scheme 3, top). Under these conditions, we could

Scheme 3. Deuterium Migration, Kinetic Isotopic Effect and Crossover Experiments

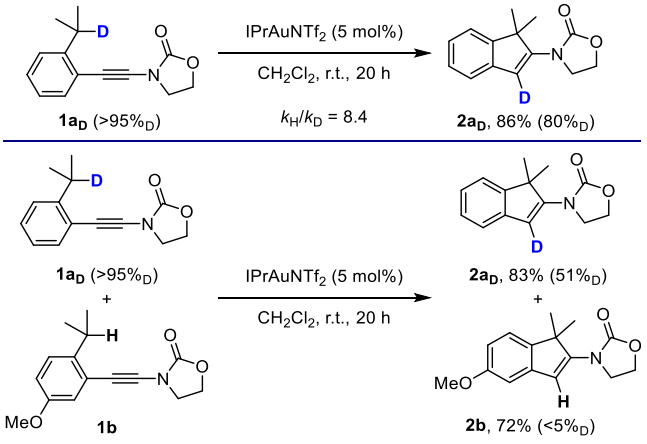

mostly observe a migration of the deuterium atom from the benzylic position to the double bond in the corresponding indene $\mathbf{2a_D}$ that was obtained with 80% deuteration, the partial loss of deuterium most certainly arising from a gold-catalyzed hydrogen/deuterium exchange from the aromatic to the vinylic positions after the cyclization since the level of deuteration is not affected by traces of water. In any case, and despite the partial loss of deuterium, the cyclization of $\mathbf{1a_D}$ to $\mathbf{2a_D}$ confirms the migration of the hydrogen atom at the benzylic position in the starting ynamide, this hydrogen atom being found on the alkene moiety in the indene resulting from the intramolecular hydroalkylation. Comparing the rates of the hydroalkylation from **1a** and $\mathbf{1a_D}$ moreover revealed a kinetic isotopic effect of 8.4.

To confirm the intramolecular nature of this deuterium shift, we next performed a crossover experiment by reacting a mixture of deuterated and undeuterated ynamides $\mathbf{1a_D}$ and **1b** under our optimized conditions (Scheme 3, bottom). The corresponding indenes $\mathbf{2a_D}$ and **2b** could be separated by flash chromatography and hence carefully analyzed for their deuterium contents. Here again, a loss of deuterium was observed from $\mathbf{1a_D}$, which can be rationalized as above, but the absence of deuterium in **2b** strongly supports the intramolecular nature of the [1,5]-hydride shift.

https://doi.org/10.1021/acsomega.4c09973
ACS Omega 2024, 9, 51690−51700

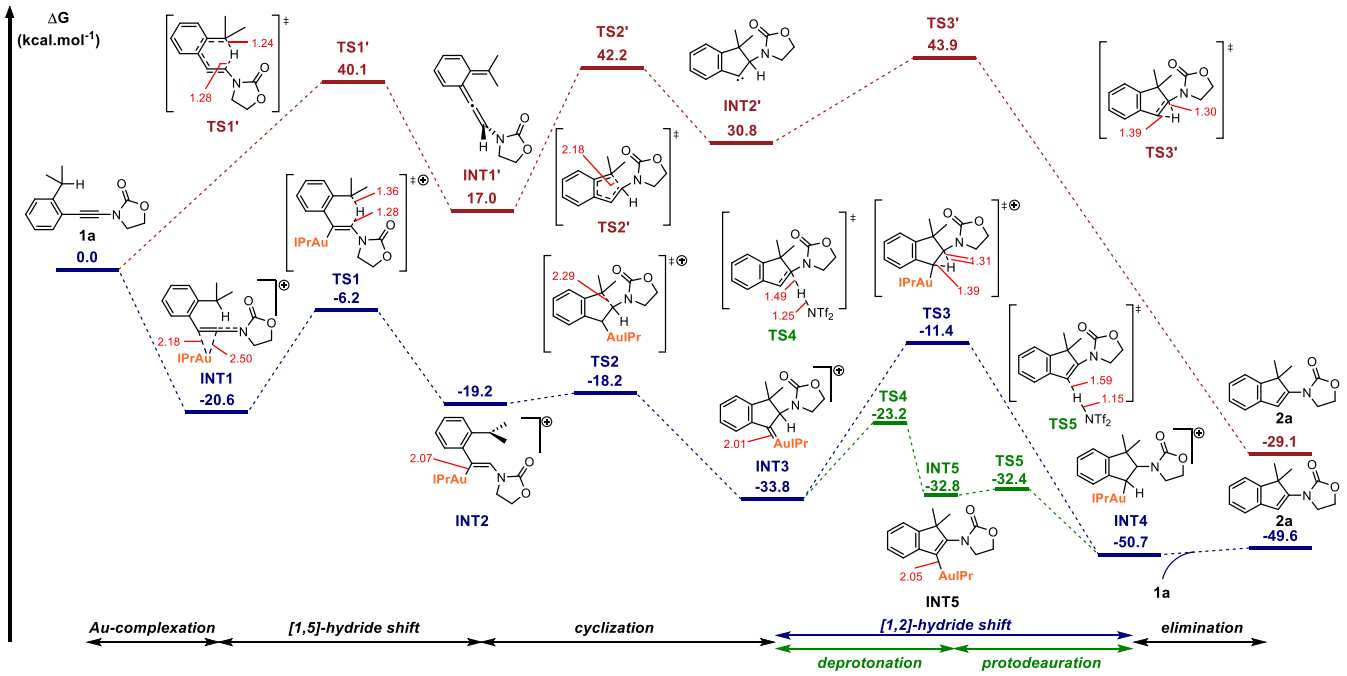

Figure 1. Relative Gibbs free energies (in kcal/mol) of the intermediates for the gold-catalyzed (blue and green pathways) and noncatalyzed (red pathway) cyclization of ynamides to indenes. Bond distances given in Å.

With this important information at our disposal, we next focused our efforts in getting additional insights into the mechanism of the gold-catalyzed intramolecular hydroalkylation of ynamides, notably through extensive computational studies.

Computational Studies for the Overall Mechanistic Pathway. To get a deeper understanding of the reaction mechanism and the factors governing the reactivity of the gold-catalyzed intramolecular hydroalkylation of ynamides, DFT calculations were performed with the Gaussian 09 software package using the B3LYP functional augmented with a damped empirical dispersion term (D3) using the solvation model (SMD) with dichloromethane (DCM) as solvent. The SDD basis set (Stuttgart/Dresden ECP) was used for Au and this basis is augmented by an additional f-type polarization function for Au with ζ = 1.050. The standard 6-311+G(d,p) basis set was used for all other atoms. The gold catalyzed intramolecular hydroalkylation of ynamide **1a** using $IPrAuNTf_2$ as the gold catalyst was selected as the model reaction for these studies. Similar studies have shown that the anion has a little impact on the reaction,[16] and thus, cationic $IPrAu^+$ was employed as the active catalyst in this study (Figure S22). All Gibbs free energies are relative to the energy of $IPrAu^+$ and **1a**.

We initially focused on the elucidation of the general reaction mechanism, which, as mentioned above, supposedly involves five pivotal steps: (a) a complexation of the gold-catalyst with the starting ynamide, (b) a [1,5]-hydride shift, (c) a cyclization event, d) a [1,2]-hydride shift[17] and (e) a final elimination of the gold(I) catalyst or, alternatively for the last two steps, (d') the loss of a proton followed by (e') protodeauration. The catalytic intramolecular hydroalkylation of ynamide **1a** starts with the complexation of $IPrAu^+$ to **1a**, generating gold-keteniminium ion **INT1**, with an exergonicity of 20.6 kcal/mol and characterized by Au−C bond distances of 2.18 and 2.50 Å. The natural bond orbital (NBO)[18] analysis revealed a bond order of 1.231 for the C−N bond in **INT1** in contrast to 1.084 for ynamide **1a** (1.31 vs 1.35 Å),[19] highlighting a partial "iminium" nature of **INT1** (see Table S1). Gold-keteniminium ion **INT1** then undergoes a [1,5]-hydride shift via **TS1**, with an activation barrier of 14.4 kcal/mol, leading to benzylic carbocationic gold adduct **INT2**. A closer look at **TS1** reveals that the length of the C···H bond being broken changes from 1.09 Å in **INT1** to 1.36 Å in **TS1**, whereas the length of the C···H bond being formed is 1.28 Å, the charge distribution in **INT2** being moreover more consistent with a [1,5]-hydride shift rather than a [1,5]-hydrogen shift. Another plausible route from **INT1** involving a [1,4]-hydride shift was also investigated but it was found to be less favorable by 11.2 kcal/mol, thus showing the [1,5]-hydride shift as the preferential pathway and rationalizing the selectivity observed experimentally. The Gibbs free energy of activation needed for the [1,5]-hydride shift in the absence of the gold catalyst (red pathway in Figure 1) via **TS1'** was shown to be as high as 40.1 kcal/mol, suggesting that this pathway is not possible kinetically and highlighting the key role of the catalyst for this transformation. C···H bond breaking and forming distances for the uncatalyzed [1,5]-hydride shift (**TS1'**) were found to be 1.24 and 1.28 Å, respectively. Regarding the catalytic process, a subsequent cyclization of carbocationic intermediate **INT2** by intramolecular addition of the vinyl-gold moiety to the tertiary carbocation results in the formation of the five-membered ring in **INT3** via **TS2**, with a very low activation Gibbs free energy of 1.0 kcal/mol. For this step, the distance between the two carbon atoms between which a bond is being formed is of 2.29 Å in **TS2**, and the resulting bicyclic intermediate **INT3** is formed exergonically by 15.6 kcal/mol. The low-energy-demanding and exergonic cyclization step drives the reaction and overcomes the slightly endergonic [1,5]-hydride shift. After cyclization, a slight change in the length of the Au−C bond could be noted, this length being of 2.07 Å before the cyclization and shortened to 2.01 Å in **INT3**. Following this cyclization, **INT3** could undergo a [1,2]-

https://doi.org/10.1021/acsomega.4c09973
ACS Omega 2024, 9, 51690−51700

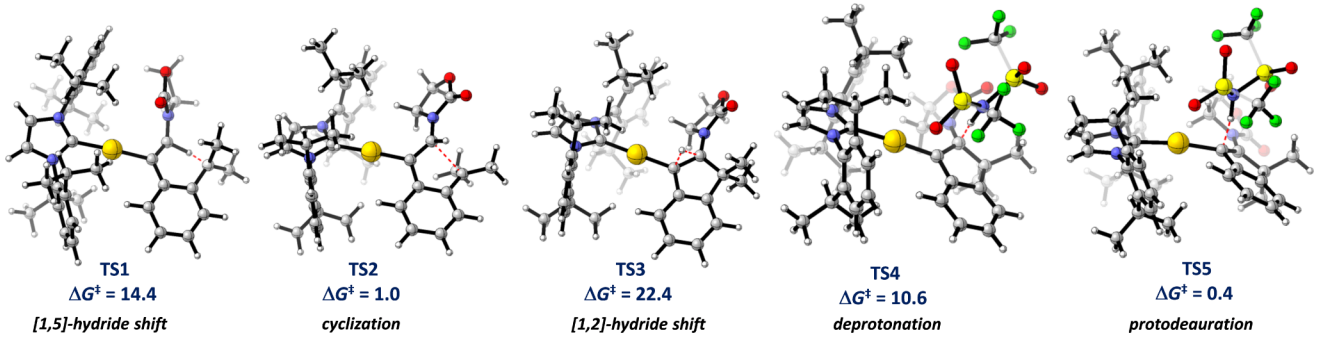

Figure 2. Optimized calculated geometries for the transition states involved in the gold-catalyzed cyclization process. Relative Gibbs free energies given in kcal/mol.

hydride shift via **TS3** with an activation Gibbs free energy of 22.4 kcal/mol to form gold-product complex **INT4**, which is the resting state of the catalytic cycle. NBO analysis revealed a bond order for the C−N bond of 0.958 in **INT4**, similar to the value of 0.949 in **INT3** (1.45 vs 1.43 Å). Alternatively, the elimination of a proton followed by protodeauration from **INT3** was also investigated. DFT calculations indicated that this process could be possible by a proton migration involving **TS4** and **TS5** facilitated by the Tf_2N^- anion. All of these intermolecular processes are quite facile via the intermediacy of **INT5**. Deprotonation of **INT3** assisted by the Tf_2N^- anion delivers **INT5** via **TS4** with an activation Gibbs free energy of 10.6 kcal/mol to form gold complex **INT5** via an almost thermoneutral step, and a subsequent protodeauration delivers the final product **2a** via **INT4**. The corresponding **TS5** was located in a very flat energy surface, and the protodeauration appeared to be practically barrierless. The protodeauration step would occur via **TS5** with a barrier of 0.4 kcal/mol, affording **INT4** with high exergonicity, and would be followed by a slightly endergonic catalyst transfer between **INT4** and substrate **1a** to yield gold−alkyne complex **INT1** and indene **2a**. Thus, according to the two possible pathways from **INT3**, i.e., the [1,2]-hydride shift and a subsequent elimination vs the elimination of the proton followed by the protodeauration, the latter would occur through a low barrier and is believed to be part of the overall mechanism of the gold-catalyzed intramolecular hydroalkylation of ynamides.

The overall Gibbs free energy change of the reaction ΔG_{rxn} is −49.6 kcal/mol (calculated from the Gibbs free energy difference between ynamide **1a** and indene **2a**). According to the Gibbs free energy profile, the reaction from **TS1** is irreversible, as all the subsequent TS are lower in energy and the reaction from **INT1** would evolve toward the low energy demanding **TS2** to deliver **INT3** in a highly exergonic step. Comparing the different elementary steps and transition states involved in this reaction (**TS1**, **TS2**, **TS4** and **TS5**, Figure 2), the [1,5]-hydride shift (**TS1**) is the rate-determining step (RDS) for the overall indene formation, which is in line with the highest computed barrier for this step ($\Delta G^{\ddagger}$ = 14.4 kcal/mol) and in agreement with the primary kinetic isotopic effect of 8.4 measured (Scheme 3, top).

For the sake of comparison, the reaction profile was also investigated using acid catalysis (Table S2), and an activation barrier of 17.2 kcal/mol was computed for the rate-determining step. This result also shows that the gold catalyst significantly favors the [1,5]-hydride shift step (energy barrier lowered by 8.5 kcal/mol), which is in adequation with the previously obtained results for the triflic acid-catalyzed reaction (52% ^{1}H NMR yield)[12] compared to the AuIPrNTf$_2$-catalyzed one (94% ^{1}H NMR yield).

Compared Reactivity of Gold Catalysts. During the optimization of the gold-catalyzed intramolecular hydroalkylation of ynamides, we noted that its efficiency was, quite logically, strongly dependent on the nature of the gold catalyst. We thus next attempted to rationalize these results by a comparative computational study for the rate-determining [1,5]-hydride shift step (**TS1**) of the reaction. N-Heterocyclic carbene (NHC)−gold complex IPrAuNTf$_2$ notably displayed a superior activity compared to that of Ph_3PAuNTf$_2$, with **2a** being obtained in 94% and 60% NMR yields, respectively (Table 1, entries 1 and 2). To investigate this difference of

Table 1. Experimental Versus Calculated Observed Reactivity of Various Gold-Complexes[a]

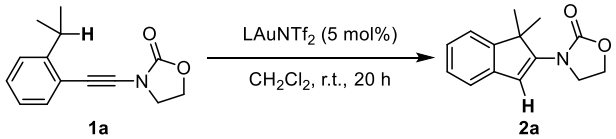

1a 2a

Entry	LAu	ΔG_{TS1} (kcal/mol)	Yield$_{exp}$ (%)[b]
1	IPrAu	14.4	94
2	Ph_3PAu	23.9	60
3	XPhosAu	12.5	97
4	JohnPhosAu	11.3	85
5	SPhosAu	12.3	82
6	MorDalPhosAu	13.5	87
7	IMesAu	14.4	93
8	BrettPhosAu	12.5	84

[a]Relative Gibbs free energies for the rate-determining [1,5]-hydride shift (**TS1**) given in kcal/mol. [b]Determined by ^{1}H NMR analysis using 1,1,2,2-tetrachloroethane as internal reference.

reactivity, both catalytic cycles were computed: as shown in Table 1, the barrier for the [1,5]-hydride shift (**TS1**) with the IPr ligand is calculated to be 14.4 kcal/mol, while it increases to 23.9 kcal/mol with triphenylphosphine as the ligand, these calculated barriers being consistent with the experimentally observed yields. The charge on the carbon atom α to the nitrogen atom in **INT1** is of 0.280 e with IPr but of −0.051 e with Ph_3P, whereas they are of 0.134 and −0.077 e at **TS1**, respectively. For the reaction involving Ph_3PAuNTf$_2$, the stronger Lewis acidic character makes the Au center more positively charged (0.331 e for Ph_3PAu^+ vs 0.298 e for IPrAu$^+$), destabilizing the transition state of the [1,5]-hydride shift. When switching to the IMes ligand, an identical energy barrier

https://doi.org/10.1021/acsomega.4c09973
ACS Omega 2024, 9, 51690−51700

profile was obtained, which is also consistent with the experimental yield obtained (93%, Table 1, entry 7). Several phosphines were also evaluated, and the corresponding Gibbs free energies of the transition states compared. In all cases studied, similar barriers were computed and the [1,5]-hydride shift step (**TS1**) was systematically found to be the rate-determining step of the overall process. Optimized structures for the rate-determining step of the process (**TS1**) of various gold-complexes at the described level of theory are shown in Table S3.

For the rest of gold complexes evaluated, the yields after 20 h at room temperature were similar, as also inferred from the comparison of the barriers observed for the computed transition states. Noteworthy, the Gibbs activation barriers can be correlated to the reaction kinetics but in our case, all reactions were performed under thermodynamic conditions, i.e., long reaction times (20 h). Thus, a correlation between reaction rates and barriers cannot be expected given that the yields obtained at 20 h are not representative of the reaction rates. This comment can be applied for all the substrates, according to the barriers we can predict that the reaction will occur or not (if the barrier is too high) but not compare reaction yields at 20 h.

Influence of the Ynamide Substitution on the 1,5-Hydride Shift. Besides the marked influence of the nature of the gold catalyst, the nature, substitution pattern and electronic properties of the starting ynamide also have an impact on the efficiency of the gold-catalyzed intramolecular hydroalkylation. In this perspective, we next focused on getting a better understanding of the influence of the nature of the starting ynamides and the prerequisites for their hydroalkylation to be operative.

The nature of the substituent at the benzylic position involved in the hydride shift was therefore investigated, both experimentally and theoretically (Scheme 4). A substituted benzylic position proved to be beneficial for the [1,5]-hydride shift of the catalytic intramolecular hydroalkylation of ynamides. Indeed, while a tertiary position such as an isopropyl (**1a**) is suitable for the hydride-shift to be operative, a secondary one such as an ethyl group (**1c**) is also suitable, resulting however in a lower yield (40%) and leading to the isomerized product. From a computational point of view, replacing the isopropyl group by an ethyl group results in an increase of the RDS barrier of 2.7 kcal/mol for the [1,5]-hydride shift step (**TS1**) and a decreasing of 5.6 kcal/mol for the deprotonation step (**TS4**). The absence of a substituent inhibited the hydroalkylation since no reaction was observed starting from *o*,*o*′-xylyl-ynamide **1d** or *o*-tolyl-ynamide **1e** which were both fully recovered at the end of the reaction. For those two ynamides **1d** and **1e**, only traces of the corresponding indenes **2d** and **2e** could be obtained when employing higher reaction temperature of 80 °C in 1,2-dichloroethane. This lack of reactivity can be rationalized from the high activation barrier of 38.0 kcal/mol for **TS1** calculated when starting from *o*,*o*′-xylyl-ynamide **1d**. For ynamide **1e**, the free activation barrier for **TS1** was found to be 23.5 kcal/mol. The methyl group in **1d** most likely forces the gold complex to bind to the alkyne with a different angle (Au−C−Ar 130° compared to 124−125° in **1a**, **1c** and **1e**, see Table S4), resulting in a more distorted TS and, hence, in a higher energy barrier. These high barriers are in line with the use of longer reaction times and higher temperatures to observe traces of **2d** and **2e**. Other ynamides having substituted tertiary positions with groups such as a cyclohexane or a cyclic acetal (not shown) showed affordable barriers similar to that of ynamide **1a**, in line with the previously experimentally observed yields.[12] For all ynamides studied, the RDS was found to be the initial [1,5]-hydride shift step and the final protodeauration step occurs with high exergonicity via **TS5**, with activation barriers lower than 1.0 kcal/mol for ynamides **1d**,**e**.

The analysis of the noncovalent interactions (NCIs) for **TS1** corresponding to the 1,5-hydride shift from compounds **1a**, **1c**, **1d** and **1e** was also performed and results are displayed in Figure 3. A clear interaction between the four isopropyl groups on the aromatic rings of the Au-NHC ligand and the gold atom can be observed. The isopropyl group in ynamide **1a** allows for a conformation in **TS1−1a** with more favorable NCI interactions compared to **TS1−1c** (Figure 3). The isosurfaces of NCI interactions were processed with an isovalue of 0.6, and showed a weak CH−π stacking interaction (with distances in the 3.30−3.40 Å range) between the phenyl ring of the substrate and phenyl of the NHC ligand for compounds **1a**, **1c** and **1e**. This CH−π stacking interaction is more favorable in **TS1−1a** and is absent in compound **1d**, which shows instead a CH_3−π stacking interaction. As ynamide **1d** has the higher barrier for **TS1**, it is believed that this CH−π stacking interaction participates in lowering the barrier for the 1,5-hydride shifts. Additionally, the incipient positive charge at the benzylic position is significantly less stabilized in **1d** (lacking the adjacent methyl groups) compared to **1a** or **1c**.

Finally, the Activation Strain Model (ASM)[20] was used to further evaluate the relative contributions of the strain and interaction terms and get insights into the influence of the ynamide substitution on the 1,5-hydride shift at **TS1**. According to this model, the optimized transition state structure is separated into two fragments (distorted ynamide and distorted gold catalyst), and the energy difference between the distorted fragments and the geometries of the fragments in

Scheme 4. Influence of the Ynamide Substitution on the Observed Reactivity; Relative Gibbs Free Energies Given in kcal/mol[a,b,c]

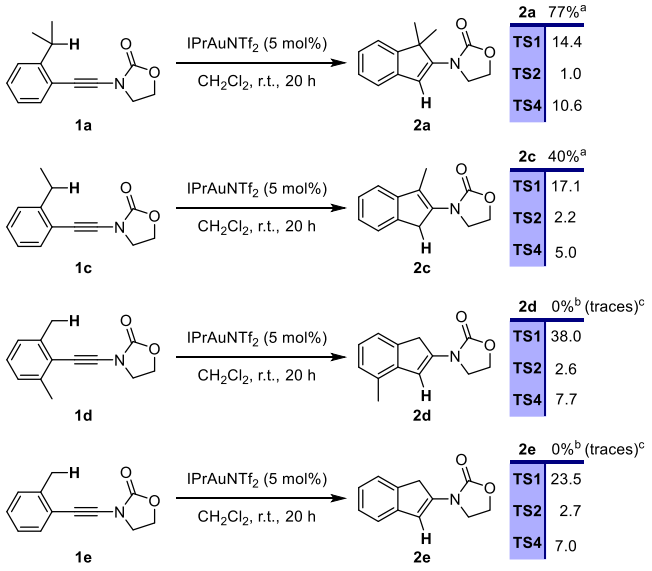

[a]Isolated yields. [b]Determined by ^{1}H NMR analysis using 1,1,2,2-tetrachloroethane as internal reference. [c]Reaction performed in 1,2-dichloroethane at 80 °C.

https://doi.org/10.1021/acsomega.4c09973
ACS Omega 2024, 9, 51690−51700

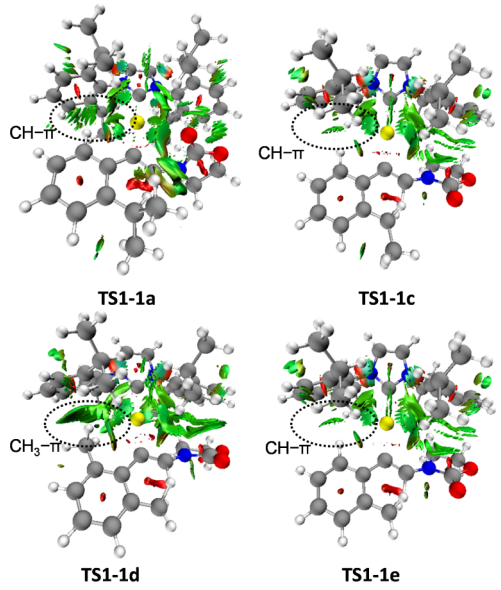

Figure 3. NCI isosurfaces (isovalue at 0.6) associated with **TS1** for compounds **1a**, **1c**, **1d** and **1e**. NCI interactions are shown in green, steric effects in red.

the initial **INT1** complex is defined as the distortion energy. The difference between the activation energy and the total distortion energy corresponds to the interaction energy. This model has been successfully applied to rationalize the reactivity of cycloadditions, substitution and elimination reactions and transition metal catalyzed reactions.[21] The corresponding values for strain energy of the ynamide ($\Delta E_{DIST(ynamide)}$), strain energy of the gold-catalyst ($\Delta E_{DIST(Au)}$), interaction energy (ΔE_{INT}) and activation energy ($\Delta E^{\ddagger}$) are shown in Figure 4. In

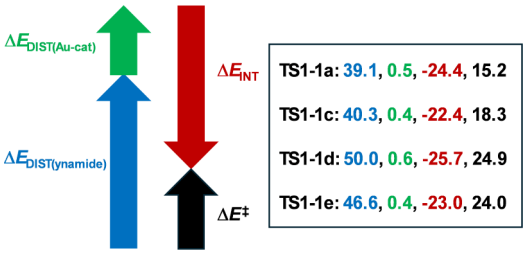

Figure 4. Analysis of distortion, interaction, and activation (blue: distortion energy of ynamides, green: distortion energy of Au-catalyst, red: interaction energy, black: activation energy). Energies are given in kcal/mol.

this case, the gold-catalyst distortion energy ($\Delta E_{DIST(Au)}$) is small and very similar for the four ynamides studied, i.e., the distortion induced by the coordination of the ynamide to the gold-catalyst does not result in significant changes in the electronic structure of the catalyst. However, significant differences can be found in the ynamide distortion energy ($\Delta E_{DIST(ynamide)}$) and its contribution to the electronic energy activation ($\Delta E^{\ddagger}$) is mainly associated with the deformation of the alkene part of the indene. Comparatively, ynamides **1a** and **1c** have similar distortion energies, while ynamides **1d** and **1e** show higher ones, and, interestingly, ynamides **1a** and **1c** have earlier TS according to H···C bond forming distances than ynamides **1d** and **1e**. The interaction energy term (ΔE_{INT}) for **TS1** remains close for all ynamides, differing only by 2−3 kcal/mol. It is slightly more stabilizing for ynamides **1a** and **1d**, being the most favorable for ynamide **1d**; however, it cannot compensate the strong destabilizing value of the total distortion energy. The higher interaction energy for **1a** and **1d** can be attributed to the oxazolidinone and the indene fragment being perpendicular and might result in a more favorable orbital interaction.

To avoid the ASM values being skewed by the position of the transition states,[22] we also performed the analyses along the reaction coordinate, in this case the C···H bond forming distance (Figure 5). Differences in the distortion energy were

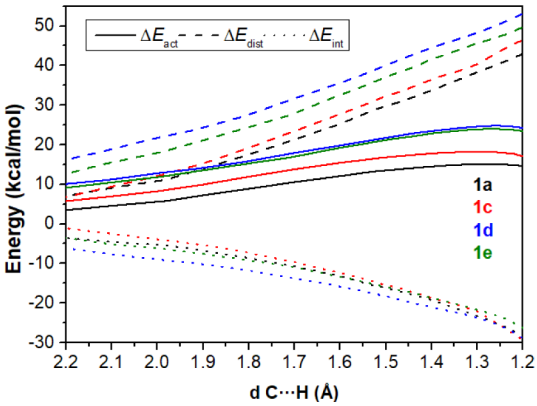

Figure 5. Activation strain diagrams for **TS1** of compounds **1a**, **1c**, **1d** and **1e** along the reaction coordinate projected onto the C···H bond stretch.

observed, the distortion energy for the reaction involving **1a** being lower along the complete reaction coordinate than for other ynamides. The variation of the interaction energy was in addition similar for the four ynamides studied. It is fairly obvious that the reactivity differences between ynamides comes from the significant differences in the distortion energy between reactants along the reaction coordinate, as both reactions show similar interaction energies. Thus, this study suggests thar the reactivity is mainly controlled by the distortion energy.

CONCLUSIONS

In conclusion, a combined experimental and computational approach enabled to elucidate the mechanism associated with the gold-catalyzed intramolecular hydroalkylation of ynamides to 2-aminoindenes. This process involves a highly reactive gold-keteniminium ion, which significantly lowers the Gibbs free energy barriers required for the first step of this reaction, i.e., the [1,5]-hydride shift from the benzylic position. The latter, occurring before the cyclization event, was identified to be the rate-determining step of the reaction. The substitution pattern of the benzylic position of the starting ynamide was also proven to be critical for the [1,5]-hydride shift, lower energy barriers being correlated with a substituted and electron-rich benzylic position. This study should hopefully guide more rational approaches for the design and the development of reactions involving keteniminium ions starting from readily available and versatile ynamides.

EXPERIMENTAL SECTION

General Information. All reactions were carried out in oven-dried glassware under an argon atmosphere employing standard techniques in handling air-sensitive materials.

https://doi.org/10.1021/acsomega.4c09973
ACS Omega 2024, 9, 51690−51700

All solvents were reagent grade. Dichloromethane was freshly distilled from calcium hydride under argon. Tetrahydrofuran was freshly distilled from sodium/benzophenone under argon. 1,4-Dioxane and DMF were used from commercially available argon-filled sealed bottles with molecular sieves.

[1,3-Bis(2,6-diisopropylphenyl)imidazol-2-ylidene][bis(trifluoromethanesulfonyl)imide]gold(I) ($IPrAuNTf_2$) (95% purity), (2-dicyclohexylphosphino-2′,4′,6′-triisopropylbiphenyl)[bis(trifluoromethanesulfonyl)imide]-gold(I) ($XPhosAuNTf_2$) (95% purity), [2-(di-*tert*-butylphosphino)biphenyl][bis(trifluoromethanesulfonyl)-imide]gold(I) ($JohnPhosAuNTf_2$) (97% purity), and $Ph_3PAuNTf_2$ (95% purity) were purchased from Merck and used as supplied. (2-Dicyclohexylphosphino-2′,6′-dimethoxybiphenyl)[bis(trifluoromethanesulfonyl)imide]gold-(I) ($SPhosAuNTf_2$) (98% purity) and [di(1-adamantyl)-2-morpholinophenylphosphine][bis(trifluoromethanesulfonyl)-imide]gold(I) ($MorDalPhosAuNTf_2$) (95% purity) were purchased from Strem Chemicals and used as supplied. [2-(Dicyclohexylphosphino)-3,6-dimethoxy-2′,4′,6′-triisopropyl-1,1′-biphenyl][bis(trifluoromethanesulfonyl)imide]gold(I) ($BrettPhosAuNTf_2$) and [1,3-bis(2,4,6-trimethylphenyl)-imidazol-2-ylidene][bis(trifluoromethanesulfonyl)imide]gold-(I) ($IMesAuNTf_2$) were prepared according to previously reported literature procedures.[23,24]

Ynamides **1a**, **1b**, **1c**, **1d** and **1e** were prepared according to a previously described procedure.[12]

Reactions were magnetically stirred and monitored by thin layer chromatography using Merck-Kieselgel $60F_{254}$ plates. Flash chromatography was performed with silica gel 60 (particle size 35−70 μm) supplied by Merck. Yields refer to chromatographically and spectroscopically pure compounds unless otherwise stated.

Proton NMR spectra were recorded using an internal deuterium lock at ambient temperature on Bruker 300 MHz, Varian 400 MHz or Varian 600 MHz spectrometers. Internal reference of δ_H 7.26 was used for $CDCl_3$. Data are presented as follows: chemical shift (in ppm on the δ scale relative to δ_{TMS} = 0), multiplicity (*s = singlet, d = doublet, t = triplet, q = quartet, quint. = quintuplet, sext. = sextuplet, sept. = septuplet, m = multiplet, br. = broad, app. = apparent*), coupling constant (*J*/Hz) and integration. Resonances that are either partially or fully obscured are denoted obscured (obs.). Carbon-13 NMR spectra were recorded at 100 MHz using $CDCl_3$ (δ_C 77.16) as internal reference. Phosphorus-31 NMR spectra were recorded at 121 MHz using phosphoric acid (δ_P 0.00) as external reference. Fluorine-19 NMR spectra were recorded at 376 MHz using fluorobenzene (δ_F −113.15) as internal reference.

Infrared spectra were recorded on a Bruker Alpha (ATR). High-resolution mass-spectra in positive mode were recorded using a 6520 series quadrupole time-of-flight (Q-TOF) mass spectrometer (Agilent) fitted with a multimode ion source.

1-Bromo-2-(propan-2-yl-2-*d*)benzene 6.[25] To a solution of 2-(2-bromophenyl)propan-2-ol **5** (2.11 g, 9.8 mmol) in anhydrous dichloromethane (16 mL) under argon was added trifluoroacetic acid-*d* (3.8 mL, 49.2 mmol) and the resulting mixture was stirred at room temperature for 5 min before adding triethyl(silane-*d*) (2.0 mL, 12.8 mmol). The resulting mixture was stirred at room temperature for 16 h. The reaction mixture was then quenched with a 1 M aqueous solution of NaOH and extracted three times with dichloromethane. The combined organic layers were dried over $MgSO_4$, filtered and concentrated under reduced pressure. The crude residue was finally purified by flash column chromatography over silica gel (petroleum ether) to afford an inseparable mixture of desired product **6** and side-product resulting from elimination **7** (**6**/**7**: 70/30 ^{1}H NMR ratio) (1.38 g). For the second step, *meta*-chloroperbenzoic acid (70% w/w, 779 mg, 3.2 mmol) then solid sodium hydrogen carbonate (355 mg, 4.2 mmol) were added to a solution of the previously obtained mixture of **6** and **7** in anhydrous dichloromethane (11 mL) under argon. The resulting mixture was stirred at room temperature for 16 h and was then quenched with deionized water before being extracted twice with dichloromethane. The combined organic layers were dried over $MgSO_4$, filtered and concentrated under reduced pressure. The crude residue was finally purified by flash column chromatography over silica gel (petroleum ether) to afford the desired deuterated product **6** as an oil. Yield: 40% (787 mg, 3.9 mmol), > 95%$_D$ (calculated by integration of the residual signal in the ^{1}H NMR spectrum). ^{1}H NMR (400 MHz, $CDCl_3$): δ 7.54−7.52 (m, 1H), 7.29−7.27 (m, 2H), 7.04 (ddd, *J* = 8.0, 5.7, 3.3 Hz, 1H), 1.24 (t, *J* = 1.0 Hz, 6H); ^{13}C{^{1}H} NMR (100 MHz, $CDCl_3$): δ 147.4, 132.9, 127.8, 127.8, 126.8, 124.4, 32.6 (t, *J* = 20 Hz, C−D), 22.8.; IR (neat): ν_{max} 2961, 2872, 1471, 1435, 1024, 751, 657 cm^{-1}; ESIHRMS *m*/*z* calcd for $C_9H_{10}DBrK$ $[M+K]^+$ 239.9718, found 239.9714.

2-(Propan-2-yl-2-*d*)benzaldehyde 9. To a solution of 1-bromo-2-(propan-2-yl-2-*d*)benzene **6** (700 mg, 3.5 mmol) in THF (7 mL) was added a 2 M solution of *n*-butyllithium in hexanes (1.9 mL, 3.9 mmol) dropwise at −78 °C under argon. The resulting mixture was then stirred at −78 °C for 30 min before adding DMF (408 μL, 5.3 mmol) dropwise. The resulting mixture was then allowed to slowly warm up to room temperature and further stirred for 1 h. The reaction mixture was then quenched with deionized water and extracted three times with diethyl ether. The combined organic layers were dried over $MgSO_4$, filtered and concentrated under reduced pressure. The crude residue was finally purified by flash column chromatography over silica gel (petroleum ether/EtOAc: 98/2) to afford the desired product **9** as a colorless liquid. Yield: 92% (481 mg, 3.2 mmol), > 95%$_D$ (calculated by integration of the residual signal in the ^{1}H NMR spectrum). ^{1}H NMR (400 MHz, $CDCl_3$): δ 10.36 (s, 1H), 7.82 (dd, *J* = 7.7, 1.5 Hz, 1H), 7.56 (dd, *J* = 7.7, 1.7 Hz, 1H), 7.46 (dd, *J* = 7.9, 1.1 Hz, 1H), 7.35 (td, *J* = 7.5, 1.2 Hz, 1H), 1.30 (t, *J* = 0.8 Hz, 6H); ^{13}C{^{1}H} NMR (100 MHz, $CDCl_3$): δ 192.5, 151.5, 134.2, 133.1, 131.7, 126.3, 126.2, 27.4 (t, *J* = 20 Hz, C−D), 23.9; IR (neat): ν_{max} 2960, 2872, 1691, 1600, 1461, 1250, 1196, 757 cm^{-1}; ESIHRMS *m*/*z* calcd for $C_{10}H_{12}DO$ $[M + H]^+$ 150.1024, found 150.1019.

1-(2,2-Dibromovinyl)-2-(propan-2-yl-2-*d*)benzene 10. To a solution of tetrabromomethane (2.12 g, 6.4 mmol) in dichloromethane (20 mL) under argon was added a solution of triphenylphosphine (3.15 g, 12.0 mmol) dropwise using an addition funnel at 0 °C for 30 min (the reaction medium progressively turned orange). A solution of aldehyde **9** (400 mg, 2.7 mmol) in dichloromethane (5 mL) was then added to the reaction mixture at 0 °C, and the mixture was allowed to warm up to room temperature and stirred for 3 h (precipitation in the reaction medium quickly occurs). Petroleum ether was then added and the reaction mixture was next filtered over a plug of Celite, rinsed with petroleum ether, and the filtrate was concentrated under reduced pressure to afford the desired product **10**, that could be used for the next step without further purification, as a clear liquid. Yield:

https://doi.org/10.1021/acsomega.4c09973
ACS Omega 2024, 9, 51690−51700

77% (631 mg, 2.07 mmol), > 95%$_D$ (calculated by integration of the residual signal in the ^{1}H NMR spectrum). ^{1}H NMR (400 MHz, $CDCl_3$): δ 7.56 (s, 1H), 7.36−7.32 (m, 1H), 7.31−7.29 (m, 2H), 7.20 (ddd, J = 8.0, 6.7, 1.7 Hz, 1H), 1.22 (t, J = 0.8 Hz, 6H); ^{13}C{^{1}H} NMR (100 MHz, $CDCl_3$): δ 146.6, 137.2, 134.6, 129.2, 129.0, 125.8, 125.3, 92.2, 30.1 (t, J = 19 Hz, C−D), 23.3; IR (neat): ν_{max} 2959, 2835, 1479, 1258, 1083, 885, 856, 795, 754 cm^{-1}; ESIHRMS m/z calcd for $C_{11}H_{12}DBr_2^+$ $[M + H]^+$ 305.9421, found 305.9425.

3-{[2-(Propan-2-yl-2-*d*)phenyl]ethynyl}oxazolidin-2-one 1a$_D$. A 15 mL oven-dried pressure tube was charged with dibromoalkene **10** (492 mg, 1.61 mmol), oxazolidine-2-one (93 mg, 1.07 mmol), copper iodide (25 mg, 0.13 mmol), *N*,*N*′-dimethylethylene-1,2-diamine (210 μL, 0.19 mmol) and cesium carbonate (1.4 g, 4.28 mmol). The tube was fitted with a rubber septum, evacuated under high vacuum and backfilled with argon three times. Anhydrous dioxane (3 mL) was next added, the rubber septum was replaced by a Teflon-coated screw cap and the resulting suspension was stirred at 80 °C for 72 h. The reaction mixture was then cooled down to room temperature, filtered over a plug of Celite, rinsed with EtOAc, and the filtrate was concentrated under reduced pressure. The crude residue was finally purified by flash column chromatography over silica gel (petroleum ether/EtOAc: 80/20) to afford the desired product **1a$_D$** as a clear oil. Yield: 40% (99 mg, 0.43 mmol), > 95%$_D$ (calculated by integration of the residual signal in the ^{1}H NMR spectrum). ^{1}H NMR (400 MHz, $CDCl_3$): δ 7.43−7.39 (m, 1H), 7.30−7.25 (m, 2H), 7.12 (ddd, J = 7.7, 5.6, 3.1 Hz, 1H), 4.52−4.48 (m, 2H), 4.04−4.00 (m, 2H), 1.26 (s, 6H); ^{13}C{^{1}H} NMR (100 MHz, $CDCl_3$): δ 155.9, 150.4, 132.3, 128.7, 125.6, 125.1, 121.0, 82.4, 70.1, 63.1, 47.2, 31.3 (t, J = 20 Hz, C−D), 23.1; IR (neat): ν_{max} 2988, 1748, 1565, 1550, 1470, 1404, 1231, 1115, 1099, 744, 643 cm^{-1}; ESIHRMS m/z calcd for $C_{14}H_{15}DNO_2$ $[M + H]^+$ 231.1238, found 231.1236.

[2-(Di-*tert*-butylphosphino)-2′,4′,6′-triisopropyl-3,6-dimethoxy-1,1′-biphenyl][bis(trifluoromethanesulfonyl)imide]gold(I) (^{t}BuBrettPhosAuNTf$_2$). A suspension of 2-(di-*tert*-butylphosphino)-2′,4′,6′-triisopropyl-3,6-dimethoxy-1,1′-biphenyl (^{t}BuBrettPhos, 268 mg, 0.5 mmol) and $AuCl(SMe)_2$ (147 mg, 0.5 mmol) in anhydrous dichloromethane (2.5 mL) under argon was stirred at room temperature for 1 h. The reaction mixture was then concentrated under reduced pressure to afford the desired intermediate chloride gold complex, pure enough to be used as such without further purification, as a white solid. Yield: quantitative (385 mg, 0.5 mmol). The crude complex (179 mg, 0.25 mmol) was then added to a solution of silver bis(triflimide) (97 mg, 0.25 mmol) in dichloromethane (5 mL) under argon and the resulting mixture was stirred at room temperature in the dark for 1 h. The reaction medium was then filtered over a plug of Celite, rinsed with dichloromethane, and the filtrate was concentrated under reduced pressure to afford the desired gold bis(triflimide) complex that can be used without further purification, as a white solid. Yield: quantitative (65 mg, 0.25 mmol). Mp: 188 °C; ^{1}H NMR (400 MHz, $CDCl_3$): δ 7.03 (s, 2H), 7.00 (d, J = 9.1 Hz, 1H), 6.94 (dd, J = 9.0, 3.3 Hz, 1H), 3.83 (s, 3H), 3.52 (s, 3H), 3.00 (sept., J = 6.9 Hz, 1H), 2.34 (sept., J = 6.7 Hz, 2H), 1.43 (s, 9H), 1.39 (s, 9H), 1.28 (obs. d, 6H), 1.28 (d, J = 6.7 Hz, 6H), 0.86 (d, J = 6.6 Hz, 6H); ^{13}C{^{1}H} NMR (100 MHz, $CDCl_3$): δ 154.6, 153.4 (d, J = 12 Hz), 149.9, 146.2, 139.8 (d, J = 16 Hz), 130.9 (d, J = 8 Hz), 122.1, 119.5 (d, J = 38 Hz), 113.8, 109.1 (d, J = 5 Hz), 54.7, 54.2, 40.4 (d, J = 26 Hz), 40.3, 34.1, 32.5 (d, J = 8 Hz), 31.0, 25.4, 24.5, 24.3; ^{31}P NMR{^{1}H} (121 MHz, $CDCl_3$): δ 70.3; ^{19}F NMR (376 MHz, $CDCl_3$): δ −76.1; IR (neat): ν_{max} 2959, 1416, 1235, 1190, 1129, 949, 614 cm^{-1}; ESIHRMS m/z calcd for $C_{33}H_{49}AuF_6NO_6PS_2$ $[M]^+$ 961.2303, found 961.2253.

General Procedure for the Gold-Catalyzed Cyclization of Ynamides to Indenes. An oven-dried 5 mL round-bottom flask was charged with the ynamide (250 μmol) and gold-complex catalyst (5 mol %, 13 μmol) and fitted with a rubber septum before being evacuated under high vacuum and backfilled with argon three times. Freshly distilled dichloromethane (3 mL) was next added, and the resulting mixture was stirred at room temperature for 20 h. The reaction mixture was then concentrated under reduced pressure and the resulting crude residue was analyzed by ^{1}H NMR after addition of an internal standard (1,1,2,2-tetrachloroethane, 0.5 equiv., 13 μL) and/or finally purified by flash column chromatography over silica gel to afford the desired 2-aminoindene.

2-(2-Oxooxazolidin-3-yl)-1,1-dimethyl-1*H*-indene 2a. Prepared according to general procedure using IPrAuNTf$_2$ (22 mg) as catalyst and ynamide **1a** (115 mg, 500 μmol). Yield: 77% (88 mg, 384 μmol). Solvent system for flash column chromatography: petroleum ether/EtOAc: 80/20. Pale yellow solid. Mp: 104 °C; ^{1}H NMR (400 MHz, $CDCl_3$): δ 7.25−7.12 (m, 4H), 6.34 (s, 1H), 4.50−4.45 (m, 2H), 4.07−4.01 (m, 2H), 1.56 (s, 6H); ^{13}C{^{1}H} NMR (100 MHz, $CDCl_3$): δ 154.9, 151.3, 151.0, 140.0, 126.9, 124.8, 120.9, 120.5, 114.2, 61.8, 49.8, 46.8, 24.0; IR (neat): ν_{max} 2962, 2926, 2869, 1747, 1564, 1470, 1403, 1343, 1263, 1212, 1114, 1052, 745, 644 cm^{-1}; ESIHRMS m/z calcd. for $C_{14}H_{16}NO_2$ $[M + H]^+$ 230.1176, found 230.1177.

2-(2-Oxooxazolidin-3-yl)-1,1-dimethyl-1*D*-indene 2a$_D$. Prepared according to general procedure using IPrAuNTf$_2$ (11 mg) as catalyst and ynamide **1a$_D$** (58 mg, 250 μmol). Yield: 87% (50 mg, 217 μmol), 80%$_D$ (calculated by integration of the residual signal in the ^{1}H NMR). Solvent system for flash column chromatography: petroleum ether/EtOAc: 80/20; White solid. Mp: 83 °C; ^{1}H NMR (400 MHz, $CDCl_3$): δ 7.24−7.22 (m, 1H), 7.21−7.17 (m, 2H), 7.16−7.12 (m, 1H), 6.35 (s, 0.2H), 4.49−4.45 (m, 2H), 4.05−4.01 (m, 2H), 1.55 (s, 6H); ^{13}C{^{1}H} NMR (100 MHz, $CDCl_3$): δ 154.9, 151.1, 150.9, 139.9, 126.8, 124.7, 120.8, 120.4, 113.8 (t, J = 26 Hz, C−D), 61.8, 49.7, 46.7, 23.9; IR (neat): ν_{max} 2964, 2869, 2256, 1770, 1479, 1203, 1095, 1034, 756 cm^{-1}; ESIHRMS m/z calcd for $C_{14}H_{15}DO_2$ $[M + H]^+$ 231.1238, found 231.1236.

2-(2-Oxooxazolidin-3-yl)-5-methoxy-1,1-dimethyl-1*H*-indene 2b. Prepared according to general procedure using IPrAuNTf$_2$ (9 mg) as catalyst and ynamide **1b** (52 mg, 200 μmol). Yield: 85% (44 mg, 170 μmol). Solvent system for flash column chromatography: petroleum ether/EtOAc: 80/20. Off-white solid. Mp: 155 °C; ^{1}H NMR (400 MHz, $CDCl_3$): δ 7.11 (d, J = 8.2 Hz, 1H), 6.77 (d, J = 2.4 Hz, 1H), 6.68 (dd, J = 8.2 and 2.4 Hz, 1H), 6.32 (s, 1H), 4.49−4.45 (m, 2H), 4.06−4.01 (m, 2H), 3.80 (s, 3H), 1.52 (s, 6H); ^{13}C{^{1}H} NMR (100 MHz, $CDCl_3$): δ 159.2, 154.9, 152.2, 143.2, 141.3, 121.3, 114.0, 110.0, 106.5, 61.8, 55.6, 49.2, 46.6, 24.2; IR (neat): ν_{max} 2987, 2920, 2328, 1739, 1569, 1472, 1408, 1300, 1215, 1150, 1111, 857, 798, 623 cm^{-1}; ESIHRMS m/z calcd. for $C_{15}H_{18}NO_3$ $[M + H]^+$ 260.1281, found 260.1284.

2-(2-Oxooxazolidin-3-yl)-1-methyl-3*H*-indene 2c. Prepared according to general procedure using IPrAuNTf$_2$ (22 mg) as catalyst and ynamide **1c** (108 mg, 500 μmol). Yield:

https://doi.org/10.1021/acsomega.4c09973
ACS Omega 2024, 9, 51690−51700

40% (43 mg, 200 μmol). Solvent system for flash column chromatography: petroleum ether/EtOAc: 80/20. Pale green solid. Mp: 117 °C; ^{1}H NMR (400 MHz, $CDCl_3$): δ 7.37 (d, J = 7.3 Hz, 1H), 7.33−7.27 (m, 2H), 7.23−7.16 (m, 1H), 4.52−4.46 (m, 2H), 4.05−3.99 (m, 2H), 3.63 (app. q, J = 1.9 Hz, 2H), 2.13 (t, J = 2.0 Hz, 3H); ^{13}C{^{1}H} NMR (100 MHz, $CDCl_3$): δ 156.1, 145.3, 139.4, 135.7, 128.8, 126.6, 125.0, 123.4, 118.9, 62.4, 46.9, 37.4, 10.9; IR (neat): ν_{max} 2925, 2868, 1740, 1471, 1403, 1359, 1225, 1205, 1115, 1086, 1035, 752, 717 cm^{-1}; ESIHRMS m/z calcd. for $C_{13}H_{17}N_2O_2$ $[M + NH_4]^+$ 233.1285, found 233.1286.

Computational Details. All DFT-calculations were performed using Gaussian 09, Revision D.01.[26] The geometry optimization and frequency analysis were performed using the B3LYP functional augmented with a damped empirical dispersion term (D3).[27] The SDD basis set (Stuttgart/Dresden ECP) was used for Au and this basis is augmented by an additional f-type polarization function for Au with ζ = 1.050.[28] The standard 6-311+G(d,p) basis set was used for all other atoms.[29] In all cases, the default integral grid (Ultrafine Grid) was employed. Frequency calculations were performed in order to obtain thermal corrections (298 K) and to confirm the nature of the stationary points (minima with no imaginary frequency or transition states with one imaginary frequency). All transition states were optimized using the default Berny algorithm implemented in the Gaussian 16 code.[30] For transition state structures, IRC calculations were undertaken to confirm that the transition states were connected to the correct minima.[31] The solvent effects (dichloromethane) were evaluated implicitly by a self-consistent reaction field (SCRF) approach for all the intermediates and transition states, using the SMD continuum solvation model.[32] Unless specified otherwise, ΔG was used throughout the text. The geometries were realized using CYLview20, Build 0001.[33] Noncovalent interactions analysis was performed using the Multiwfn program[34] and visualized by visual molecular dynamics software (VMD).[35] Validation of the computational model and method was done for the key step. Calculations of relative solvation Gibbs free energies were done with different DFT functionals (wB97xD, M06-2X and BP86) and yielded similar barriers (see Table S5).

■ ASSOCIATED CONTENT

Supporting Information

The Supporting Information is available free of charge at https://pubs.acs.org/doi/10.1021/acsomega.4c09973.

Experimental procedures, characterization, copies of H, ^{13}C, ^{19}F and ^{31}P spectra for all new compounds (PDF)

Computational details (XYZ)

■ AUTHOR INFORMATION

Corresponding Authors

Jorge Escorihuela − *Departamento de Química Orgánica, Universitat de València, Burjassot, València 46100, Spain;* orcid.org/0000-0001-6756-0991; Email: jorge.escorihuela@uv.es

Gwilherm Evano − *Laboratoire de Chimie Organique, Service de Chimie et PhysicoChimie Organiques, Université libre de Bruxelles (ULB), Brussels 1050, Belgium; WEL Research Institute, Wavre 1300, Belgium;* orcid.org/0000-0002-2939-4766; Email: gwilherm.evano@ulb.be

Authors

Julien Annibaletto − *Laboratoire de Chimie Organique, Service de Chimie et PhysicoChimie Organiques, Université libre de Bruxelles (ULB), Brussels 1050, Belgium*

Clément Jacob − *Laboratoire de Chimie Organique, Service de Chimie et PhysicoChimie Organiques, Université libre de Bruxelles (ULB), Brussels 1050, Belgium; Organic Synthesis Division, Department of Chemistry, University of Antwerp, Antwerp 2020, Belgium*

Pierre Thilmany − *Laboratoire de Chimie Organique, Service de Chimie et PhysicoChimie Organiques, Université libre de Bruxelles (ULB), Brussels 1050, Belgium*

Anaïs Loison − *Laboratoire de Chimie Organique, Service de Chimie et PhysicoChimie Organiques, Université libre de Bruxelles (ULB), Brussels 1050, Belgium*

Complete contact information is available at: https://pubs.acs.org/10.1021/acsomega.4c09973

Notes

The authors declare no competing financial interest.

■ ACKNOWLEDGMENTS

Our work was supported by the Federal Excellence of Science (EoS) program (BIOFACT, Grant No. O019618F), the FNRS (GEQ2011-2.5014.12), FWO WOG, and the Université libre de Bruxelles (ULB). P.T. acknowledges the Fonds pour la Formation à Recherche dans l'Industrie et dans l'Agriculture (F.R.I.A.) for a graduate fellowship. The computational resources from the Servei d'Informàtica de la Universidad de Valencia (SIUV) are gratefully acknowledged for providing access to supercomputing resources. We thank the Centre d'Instrumentation en Résonance Magnétique - CIREM (ULB) for providing support and access to its infrastructure. Pr. Fabien Gagosz (University of Ottawa) is gratefully acknowledged for useful discussions.

■ REFERENCES

(1) Herdman, C. A.; Strecker, T. E.; Tanpure, R. P.; Chen, Z.; Winters, A.; Gerberich, J.; Liu, L.; Hamel, E.; Mason, R. P.; Chaplin, D. J.; Trawick, M. L.; Pinney, K. G. Synthesis and Biological Evaluation of Benzocyclooctene-Based and Indene-Based Anticancer Agents that Function as Inhibitors of Tubulin Polymerization. *Med. Chem. Commun.* **2016**, *7*, 2418−2427.

(2) (a) El-Sheshtawy, H.-S.; Baker, A. M. A. Synthesis, Structural, Theoretical Studies and Biological Activities of 3-(arylamino)-2-phenyl-1*H*-inden-1-one Derivative. *J. Mol. Struct.* **2014**, *1067*, 225−232. (b) Kahlon, A. K.; Negi, A. S.; Kumari, R.; Srivastava, K. K.; Kumar, S.; Darokar, M. P.; Sharma, A. Identification of 1-chloro-2-formyl Indenes and Tetralenes as Novel Antistaphylococcal Agents Exhibiting Sortase A Inhibition. *Appl. Microbiol. Biotechnol.* **2014**, *98*, 2041−2051. (c) Chanda, D.; Saikia, D.; Kumar, J. K.; Thakur, J. P.; Agarwal, J.; Chanotiya, C. S.; Shanker, K.; Negi, A. S. 1-Chloro-2-formyl Indenes and Tetralenes as Antitubercular Agents. *Bioorg. Med. Chem. Lett.* **2011**, *21*, 3966−3969.

(3) Tu, S.; Xu, L.-H.; Ye, L.-Y.; Wang, X.; Sha, Y.; Xiao, Z.-X. Synthesis and Fungicidal Activities of Novel Indene-Substituted Oxime Ether Strobilurins. *J. Agric. Food Chem.* **2008**, *56*, 5247−5253.

(4) Selected recent examples: (a) Cao, T.; Chen, N.; Liu, G.; Wan, Y.; Perea, J. D.; Xia, Y.; Wang, Z.; Song, B.; Li, N.; Li, X.; Zhou, Y.; Brabec, C. J.; Li, Y. Towards a Full Understanding of Regioisomer Effects of Indene-C60 Bisadduct Acceptors in Bulk Heterojunction Polymer Solar Cells. *J. Mater. Chem. A* **2017**, *5*, 10206−10219. (b) Xu, X.; Li, Z.; Wang, Z.; Li, K.; Feng, K.; Peng, Q. 10.20% Efficiency polymer solar cells via employing bilaterally hole-cascade diazaphenanthrobisthiadiazole polymer donors and electron-cascade

indene-C70 bisadduct acceptor. *Nano Energy* **2016**, *25*, 170−183. (c) Dang, J.-S.; Wang, W.-W.; Zhao, X.; Nagase, S. Regioselective Derivatization of C84 by Diels−Alder Reactions: Applications to Photovoltaic Solar Cells and Fullerene Polymerization. *Org. Lett.* **2014**, *16*, 170−173. (d) Shoaee, S.; Subramaniyan, S.; Xin, H.; Keiderling, C.; Tuladhar, P. S.; Jamieson, F.; Jenekhe, S. A.; Durrant, J. R. Charge Photogeneration for a Series of Thiazolo-Thiazole Donor Polymers Blended with the Fullerene Electron Acceptors PCBM and ICBA. *Adv. Funct. Mater.* **2013**, *23*, 3286−3298. (e) Kang, H.; Cho, C.-H.; Cho, H.-H.; Kang, T. E.; Kim, H. J.; Kim, K.-H.; Yoon, S. C.; Kim, B. J. Controlling Number of Indene Solubilizing Groups in Multiadduct Fullerenes for Tuning Optoelectronic Properties and Open-Circuit Voltage in Organic Solar Cells. *ACS Appl. Mater. Interfaces* **2012**, *4*, 110−116. (f) He, Y.; Chen, H.-Y.; Hou, J.; Li, Y. Indene−C60 Bisadduct: A New Acceptor for High-Performance Polymer Solar Cells. *J. Am. Chem. Soc.* **2010**, *132*, 1377−2382. (g) He, Y.; Zhao, G.; Peng, B.; Li, Y. High-Yield Synthesis and Electrochemical and Photovoltaic Properties of Indene-C70 Bisadduct. *Adv. Funct. Mater.* **2010**, *20*, 3383−3389.

(5) Xia, Z.-Y.; Zhang, Z.-Y.; Su, J.-H.; Zhang, Q.; Fung, K.-M.; Lam, M.-K.; Li, K.-F.; Wong, W.-Y.; Cheah, K.-W.; Tian, H.; Chen, C. H. Robust and Highly Efficient Blue Light-Emitting Hosts Based on Indene-Substituted Anthracene. *J. Mater. Chem.* **2010**, *20*, 3768−3774.

(6) (a) Trost, B. M.; Ryan, M. C. Indenylmetal Catalysis in Organic Synthesis. *Angew. Chem., Int. Ed.* **2017**, *56*, 2862−2879. (b) Rojo, B.; Peris, E. Cyclopentadienyl-Indenyl- and Fluorenyl-Functionalized N-Heterocyclic Carbene Metal Complexes: Synthesis and Catalytic Applications. *Eur. J. Inorg. Chem.* **2012**, 1309−1318. (c) Djukic, J.-P.; Iali, W.; Hijazi, A.; Ricard, L. Synthesis of a 2-Benzocymantrenylpyridine and Further Mechanistic Insights. *J. Organomet. Chem.* **2011**, *696*, 2101−2107. (d) Chen, D.; Zhang, X.; Xu, S.; Song, H.; Wang, B. Pyridyl-Substituted Indenyl Ruthenium Complexes: Synthesis, Structures, and Reactivities. *Organometallics* **2010**, *29*, 3418−3430. (e) Enders, M.; Baker, R. W. Synthesis of Aryl- and Heteroaryl-Substituted Cyclopentadienes and Indenes and their Use in Transition Metal Chemistry. *Curr. Org. Chem.* **2006**, *10*, 937−953. (f) Leino, R.; Lehmus, P.; Lehtonen, A. Heteroatom-Substituted Group 4 Bis(indenyl)metallocenes. *Eur. J. Inorg. Chem.* **2004**, *2004*, 3201−3222. (g) Zargarian, D. Group 10 Metal Indenyl Complexes. *Coord. Chem. Rev.* **2002**, *233*−*234*, 157−176.

(7) (a) Barrera, E. G.; Stedile, F. C.; de Souza, M. O.; Miranda, M. S. L.; de Souza, R. F.; Bernardo-Gusmao, K. Ethylene Polymerization Using Metallocene Catalyst Supported on Hybrid Indenyl Silica Produced by Sol−Gel Process. *Appl. Catal., A* **2013**, *462*, 1−7. (b) Alt, H. G.; Koppl, A. Effect of the Nature of Metallocene Complexes of Group IV Metals on Their Performance in Catalytic Ethylene and Propylene Polymerization. *Chem. Rev.* **2000**, *100*, 1205−1222. (c) McKnight, A. L.; Waymouth, R. M. Group 4 *ansa*-Cyclopentadienyl-Amido Catalysts for Olefin Polymerization. *Chem. Rev.* **1998**, *98*, 2587−2598. (d) Hlatky, G. G. Metallocene Catalysts for Olefin Polymerization: Annual Review for 1996. *Coord. Chem. Rev.* **1999**, *181* (181), 243−296. (e) Brintzinger, H. H.; Fischer, D.; Mülhaupt, R.; Rieger, B.; Waymouth, R. M. Stereospecific Olefin Polymerization with Chiral Metallocene Catalysts. *Angew. Chem. Int. Ed.* **1995**, *34*, 1143−1170.

(8) For recent reviews, see: (a) Gabriele, B.; Mancuso, R. Recent Advances in the Synthesis of Indanes and Indenes. *Chem.—Eur. J.* **2016**, *22*, 5056−5094. (b) Rinaldi, A.; Scarpi, D.; Occhiato, E. G. Recent Advances in the Synthesis of Indenes. *Eur. J. Org. Chem.* **2019**, *2019*, 7401−7419.

(9) For a review, concerning the activation of ynamides via gold catalysis, see: Shandilya, S.; Gogoi, M. P.; Dutta, S.; Sahoo, A. K. Gold-Catalyzed Transformation of Ynamides. *Chem. Rec.* **2021**, *21*, 4123−4149.

(10) For reviews, see: (a) Evano, G.; Coste, A.; Jouvin, K. Ynamides: Versatile Tools in Organic Synthesis. *Angew. Chem., Int. Ed.* **2010**, *49*, 2840−2859. (b) DeKorver, K. A.; Li, H.; Lohse, A. G.; Hayashi, R.; Lu, Z.; Zhang, Y.; Hsung, R. P. Ynamides: A Modern Functional Group for the New Millennium. *Chem. Rev.* **2010**, *110*, 5064−5106. (c) Evano, G.; Theunissen, C.; Lecomte, M. Ynamides: Powerful and Versatile Reagents for Chemical Synthesis. *Aldrichimica Acta* **2015**, *48*, 59−70. (d) Evano, G.; Jouvin, K.; Coste, A. General Amination Reactions for the Synthesis of Ynamides. *Synthesis* **2012**, *45*, 17−26. (e) *The Chemistry of Ynamides: development, Syntheses and Application in Organic Synthesis*, Evano, G.; Zhao, J., Eds.; Jenny Stanford Publishing: Singapore, 2024.

(11) For recent examples of procedures for the synthesis of aminoindenes, see: (a) Liu, C.-C.; Koviri, R. P.; Cheng, C.-H. Cobalt-Catalyzed Regioselective Synthesis of Indenamines from *o*-Iodobenzaldimine and Alkyne: Intriguing Difference to the Nickel-Catalyzed Reaction. *Chem.—Eur. J.* **2008**, *14*, 9503−9506. (b) Adcock, H. V.; Langer, T.; Davies, P. W. 1,2-*N*-Migration in a Gold-Catalysed Synthesis of Functionalised Indenes by the 1,1-Carboalkoxylation of Ynamides. *Chem.—Eur. J.* **2014**, *20*, 7262−7266. (c) Wang, S.; Zhu, Y.; Wang, Y.; Lu, P. Synthesis of Functionalized Indenes via Cascade Reaction of Aziridines and Propargylic Alcohols. *Org. Lett.* **2009**, *11*, 2615−2618. (d) Wang, X.; Xiong, W.; Huang, Y.; Zhu, J.; Hu, Q.; Wu, W.; Jiang, H. Palladium-Catalyzed Synthesis of 1*H*-Indenes and Phthalimides via Isocyanide Insertion. *Org. Lett.* **2017**, *19*, 5818−5821. (e) Querard, P.; Li, C.-J. Direct Synthesis of Indenes via a Rhodium-Catalyzed Multicomponent C(sp)2−H Annulation Reaction. *Org. Biomol. Chem.* **2018**, *16*, 8042−8047. (f) Zhang, J.; Sun, J.-S.; Xia, Y.-Q.; Dong, L. Efficient Synthesis of Functionalized Indene Derivatives via Rh(III)-Catalyzed Cascade Reaction between Oxadiazoles and Allylic Alcohols. *Adv. Synth. Catal.* **2019**, *361*, 2037−2041. (g) Lv, N.; Chen, Z.; Liu, Y.; Liu, Z.; Zhang, Y. Rhodium-Catalyzed Cascade Annulation of Benzimidates and Nitroalkenes for the Synthesis of Difunctionalized Indenes. *Adv. Synth. Catal.* **2019**, *361*, 4140−4146. (h) Jayaram, V.; Sridhar, T.; Sharma, G. V. M.; Berree, F.; Carboni, B. Synthesis of 1-Amino-1*H*-Indenes via a Sequential Suzuki−Miyaura Coupling/Petasis Condensation Sequence. *J. Org. Chem.* **2017**, *82*, 1803−1811.

(12) Thilmany, P.; Guarnieri-Ibañez, A.; Jacob, C.; Lacour, J.; Evano, G. Straightforward Synthesis of Indenes by Gold-Catalyzed Intramolecular Hydroalkylation of Ynamides. *ACS Org. Inorg. Au* **2022**, *2*, 53−58.

(13) For reviews on keteniminium ions in organic synthesis, see: (a) Theunissen, C.; Thilmany, P.; Lecomte, M.; Evano, G. Keteniminium Ions: Unique and Versatile Reactive Intermediates for Chemical Synthesis. *Synthesis* **2017**, *49*, 3183−3214. (b) Madelaine, C.; Valerio, V.; Maulide, N. Revisiting Keteniminium Salts: More than the Nitrogen Analogs of Ketenes. *Chem. − Asian J.* **2011**, *6*, 2224−2239.

(14) For literature concerning the use of keteniminiums through reactions involving hydride-shift, see: (a) Kramer, S.; Odabachian, Y.; Overgaard, J.; Rottländer, M.; Gagosz, F.; Skrydstrup, T. Taking Advantage of the Ambivalent Reactivity of Ynamides in Gold Catalysis: A Rare Case of Alkyne Dimerization. *Angew. Chem., Int. Ed.* **2011**, *50*, 5090−5094. (b) Laub, H. A.; Evano, G.; Mayr, H. Hydrocarbation of C≡C Bonds: Quantification of the Nucleophilic Reactivity of Ynamides. *Angew. Chem. Int. Ed.* **2014**, *53*, 4968−4971. (c) Theunissen, C.; Métayer, B.; Henry, N.; Compain, G.; Marrot, J.; Martin-Mingot, A.; Thibaudeau, S.; Evano, G. Keteniminium Ion-Initiated Cascade Cationic Polycyclization. *J. Am. Chem. Soc.* **2014**, *136*, 12528−12531. (d) Adcock, H. V.; Chatzopoulou, E.; Davies, P. W. Divergent C-H Insertion−Cyclization Cascades of *N*-Allyl Ynamides. *Angew. Chem. Int. Ed.* **2015**, *54*, 15525−15529. (e) Zhao, Q.; Gagosz, F. Synthesis of Allenamides and Structurally Related Compounds by a Gold-Catalyzed Hydride Shift Process. *Adv. Synth. Catal.* **2017**, *359*, 3108−3113. (f) Lecomte, M.; Evano, G. Harnessing the Electrophilicity of Keteniminium Ions: A Simple and Straightforward Entry to Tetrahydropyridines and Piperidines from Ynamides. *Angew. Chem. Int. Ed.* **2016**, *55*, 4547−4551.

(15) (a) Coste, A.; Karthikeyan, G.; Couty, F.; Evano, G. Copper-Mediated Coupling of 1,1-Dibromo-1-alkenes with Nitrogen Nucleophiles: A General Method for the Synthesis of Ynamides. *Angew. Chem. Int. Ed.* **2009**, *48*, 4381−4385. (b) Theunissen, C.;

https://doi.org/10.1021/acsomega.4c09973
ACS Omega 2024, 9, 51690−51700

Thilmany, P.; Lahboubi, M.; Blanchard, N.; Evano, G. Discussion Addendum for: Synthesis of Ynamides by Copper-Mediated Coupling of 1,1-Dibromo-1-alkenes with Nitrogen Nucleophiles. Preparation of 4-Methyl-*N*-(2-phenylethynyl)-*N*-(phenylmethyl)-benzenesulfonamide. *Org. Synth.* **2019**, *96*, 195−213.
(16) Duan, Y.; Liu, Y.; Bi, S.; Ling, B.; Jiang, Y.-Y.; Liu, P. Theoretical Study of Gold-Catalyzed Cyclization of 2-Alkynyl-*N*-propargylanilines and Rationalization of Kinetic Experimental Phenomena. *J. Org. Chem.* **2016**, *81*, 9381−9388.
(17) Wang, T.; Hashmi, S. K. 1,2-Migrations onto Gold Carbene Centers. *Chem. Rev.* **2021**, *121*, 8948−8978.
(18) Foster, J. P.; Weinhold, F. Natural hybrid orbitals. *J. Am. Chem. Soc.* **1980**, *102*, 7211−7218.
(19) Mayer, I. Bond order and valence indices: a personal account. *J. Comput. Chem.* **2007**, *28*, 204−221.
(20) Bickelhaupt, F. M.; Houk, K. N. Analyzing Reaction Rates with the Distortion/Interaction-Activation Strain Model. *Angew. Chem., Int. Ed.* **2017**, *56*, 10070−10086.
(21) (a) Fernández, I. Understanding the Reactivity of Fullerenes Through the Activation Strain Model. *Eur. J. Org. Chem.* **2018**, *2018*, 1394−1402. (b) Hansen, T.; Vermeeren, P.; de Jong, L.; Bickelhaupt, F. M.; Hamlin, T. A. S_N versus S_N' Competition. *J. Org. Chem.* **2022**, *87*, 8892−8901. (c) Hansen, T.; Roozee, J. C.; Bickelhaupt, F. M.; Hamlin, T. A. How Solvation Influences the S_N versus E2 Competition. *J. Org. Chem.* **2022**, *87*, 1805−1813. (d) Escorihuela, J.; Wolf, L. M. Computational Study on the Co-Mediated Intramolecular Pauson-Khand Reaction of Fluorinated and Chiral N-Tethered 1,7-Enynes. *Organometallics* **2022**, *41*, 2525−2534. (e) Escorihuela, J. A Density Functional Theory Study on the Cobalt-Mediated Intramolecular Pauson-Khand Reaction of Enynes Containing a Vinyl Fluoride Moiety. *Synthesis* **2023**, *55*, 1139−1149.
(22) (a) Fernández, I.; Bickelhaupt, F. M. The activation strain model and molecular orbital theory: understanding and designing chemical reactions. *Chem. Soc. Rev.* **2014**, *43*, 4953−4967. (b) Vermeeren, P.; van der Lubbe, S. C. C.; Fonseca Guerra, C.; Bickelhaupt, F.; Hamlin, T. A. Understanding chemical reactivity using the activation strain model. *Nat. Protoc.* **2020**, *15*, 649−667.
(23) For the synthesis of BrettPhosAuNTf$_2$, see: Cai, J.; Wang, X.; Qian, Y.; Qiu, L.; Ju, W.; Xu, X. Gold-Catalyzed Oxidative Cyclization/Aldol Addition of Homopropargyl Alcohols with Isatins. *Org. Lett.* **2019**, *21*, 369−372.
(24) For the synthesis of IMesAuNTf$_2$, see: Pažický, M.; Loos, A.; João Ferreira, M.; Serra, D.; Vinokurov, N.; Rominger, F.; Jäkel, C.; Hashmi, A. S. K.; Limbach, M. Synthesis, Reactivity, and Electrochemical Studies of Gold(I) and Gold(III) Complexes Supported by *N*-Heterocyclic Carbenes and Their Application in Catalysis. *Organometallics* **2010**, *29*, 4448−4458.
(25) Inspired from previously reported procedure: Dexheimer, T. S.; Rosenthal, A. S.; Luci, D. K.; Liang, Q.; Villamil, M. A.; Chen, J.; Sun, H.; Kerns, E. H.; Simeonov, A.; Jadhav, A.; Zhuang, Z.; Maloney, D. J. Synthesis and Structure−Activity Relationship Studies of *N*-Benzyl-2-phenylpyrimidin-4-amine Derivatives as Potent USP1/UAF1 Deubiquitinase Inhibitors with Anticancer Activity against Nonsmall Cell Lung Cancer. *J. Med. Chem.* **2014**, *57*, 8099−8110.
(26) Frisch, M. J.; Trucks, G. W.; Schlegel, H. B.; Scuseria, G. E.; Robb, M. A.; Cheeseman, J. R.; Scalmani, G.; Barone, V.; Petersson, G. A.; Nakatsuji, H., et al. *Gaussian 09, Revision D.01*; Gaussian, Inc.: Wallingford CT, 2013.
(27) Grimme, S.; Antony, J.; Ehrlich, S.; Krieg, H. A Consistent and Accurate ab initio Parametrization of Density Functional Dispersion Correction (DFT-D) for the 94 Elements H-Pu. *J. Chem. Phys.* **2010**, *132*, 154104.
(28) Ehlers, A. W.; Böhme, M.; Dapprich, S.; Gobbi, A.; Höllwarth, A.; Jonas, V.; Köhler, K. F.; Stegmann, R.; Veldkamp, A.; Frenking, G. A Set of f-Polarization Functions for Pseudo-Potential Basis Sets of the Transition Metals Sc−Cu, Y−Ag and La−Au. *Chem. Phys. Lett.* **1993**, *208*, 111−114.
(29) Krishnan, R.; Binkley, J. S.; Seeger, R.; Pople, J. A. Self-Consistent Molecular Orbital Methods. XX. A Basis Set for Correlated Wave Functions. *J. Chem. Phys.* **1980**, *72*, 650−654.
(30) Schlegel, H. B. Optimization of Equilibrium Geometries and Transition Structures. *J. Comput. Chem.* **1982**, *3*, 214−218.
(31) Zhao, Y.; Truhlar, D. G. The M06 Suite of Density Functionals for Main Group Thermochemistry, Thermochemical Kinetics, Noncovalent Interactions, Excited States, and Transition Elements: Two New Functionals and Systematic Testing of Four M06-Class Functionals and 12 Other Functionals. *Theor. Chem. Acc.* **2008**, *120*, 215−241.
(32) Marenich, A. V.; Cramer, C. J.; Truhlar, D. G. Universal Solvation Model Based on Solute Electron Density and on a Continuum Model of the Solvent Defined by the Bulk Dielectric Constant and Atomic Surface Tensions. *J. Phys. Chem. B* **2009**, *113*, 6378−6396.
(33) Legault, C. Y. *CYLview20*; Université de Sherbrooke, 2020. http://www.cylview.org.
(34) Lu, T.; Chen, F. Multiwfn: A multifunctional wavefunction analyzer. *J. Comput. Chem.* **2012**, *33*, 580−592.
(35) Humphrey, W.; Dalke, A.; Schulten, K. VMD: Visual molecular dynamics. *J. Mol. Graphics* **1996**, *14*, 33−38.

https://doi.org/10.1021/acsomega.4c09973
ACS Omega 2024, 9, 51690−51700